



HAL
open science

Spatially resolved images of reactive ions in the Orion Bar

Javier R. Goicoechea, S. Cuadrado, J. Pety, E. Bron, J. H. Black, J. Cernicharo, E. Chapillon, A. Fuente, Maryvonne Gerin

► **To cite this version:**

Javier R. Goicoechea, S. Cuadrado, J. Pety, E. Bron, J. H. Black, et al.. Spatially resolved images of reactive ions in the Orion Bar. *Astronomy and Astrophysics - A&A*, 2017, 601, pp.id.L9. 10.1051/0004-6361/201730716 . hal-01516644

HAL Id: hal-01516644

<https://hal.science/hal-01516644>

Submitted on 27 Mar 2024

HAL is a multi-disciplinary open access archive for the deposit and dissemination of scientific research documents, whether they are published or not. The documents may come from teaching and research institutions in France or abroad, or from public or private research centers.

L'archive ouverte pluridisciplinaire **HAL**, est destinée au dépôt et à la diffusion de documents scientifiques de niveau recherche, publiés ou non, émanant des établissements d'enseignement et de recherche français ou étrangers, des laboratoires publics ou privés.

Published in final edited form as:

Astron Astrophys. 2017 May ; 601: . doi:10.1051/0004-6361/201730716.

Spatially resolved images of reactive ions in the Orion Bar★,★★

Javier R. Goicoechea¹, Sara Cuadrado¹, Jérôme Pety^{2,3}, Emeric Bron^{1,3}, John H. Black⁴, José Cernicharo¹, Edwige Chapillon^{2,5}, Asunción Fuente⁶, and Maryvonne Gerin³

¹Instituto de Ciencias de Materiales de Madrid (CSIC), 28049, Madrid, Spain

²Institut de Radioastronomie Millimétrique, 38406, Saint Martin d'Hères, France

³LERMA, Obs. de Paris, PSL Research University, CNRS, Sorbonne Universités, UPMC Univ. Paris 06, ENS, F-75005, France

⁴Chalmers University of Technology, Onsala Space Observatory, 43992 Onsala, Sweden

⁵OASU/LAB-UMR5804, CNRS, Université Bordeaux, 33615 Pessac, France

⁶Observatorio Astronómico Nacional (IGN). Apartado 112, 28803 Alcalá de Henares, Spain

Abstract

We report high angular resolution ($4.9'' \times 3.0''$) images of reactive ions SH^+ , HOC^+ , and SO^+ toward the Orion Bar photodissociation region (PDR). We used ALMA-ACA to map several rotational lines at 0.8 mm, complemented with multi-line observations obtained with the IRAM 30 m telescope. The SH^+ and HOC^+ emission is restricted to a narrow layer of $2''$ - to $10''$ -width (≈ 800 to 4000 AU depending on the assumed PDR geometry) that follows the vibrationally excited H_2^* emission. Both ions efficiently form very close to the H/H_2 transition zone, at a depth of $A_V \lesssim 1$ mag into the neutral cloud, where abundant C^+ , S^+ , and H_2^* coexist. SO^+ peaks slightly deeper into the cloud. The observed ions have low rotational temperatures ($T_{\text{rot}} \approx 10\text{-}30 \text{ K} \ll T_k$) and narrow line-widths ($\sim 2\text{-}3 \text{ km s}^{-1}$), a factor of ≈ 2 narrower than those of the lighter reactive ion CH^+ . This is consistent with the higher reactivity and faster radiative pumping rates of CH^+ compared to the heavier ions, which are driven relatively faster toward smaller velocity dispersion by elastic collisions and toward lower T_{rot} by inelastic collisions. We estimate column densities and average physical conditions from an excitation model ($n(\text{H}_2) \approx 10^5\text{-}10^6 \text{ cm}^{-3}$, $n(e^-) \approx 10 \text{ cm}^{-3}$, and $T_k \approx 200 \text{ K}$). Regardless of the excitation details, SH^+ and HOC^+ clearly trace the most exposed layers of the UV-irradiated molecular cloud surface, whereas SO^+ arises from slightly more shielded layers.

Keywords

astrochemistry; line: identification; ISM: clouds; ISM: molecules; photon-dominated region (PDR)

★This paper makes use of the following ALMA data: ADS/JAO.ALMA#2012.1.00352.S. ALMA is a partnership of ESO (representing its member states), NSF (USA), and NINS (Japan), together with NRC (Canada), and NSC and ASIAA (Taiwan), in cooperation with the Republic of Chile. The Joint ALMA Observatory is operated by ESO, AUI/NRAO, and NAOJ.

jr.goicoechea@icmm.csic.es.

1 Introduction

Reactive ions are transient species for which the timescale of reactive collisions with H_2 , H, or e^- (leading to a chemical reaction, and thus molecule destruction) is comparable to, or shorter than, that of inelastic collisions (Black 1998; Nagy et al. 2013; Godard & Cernicharo 2013). The formation of reactive ions such as CH^+ and SH^+ depends on the availability of C^+ and S^+ (i.e., of UV photons and thus high ionization fractions $x_e = n(e^-)/n_{\text{H}}$), and on the presence of excited H_2 (either UV-pumped or hot and thermally excited). This allows overcoming the high endothermicity (and sometimes energy barrier) of some of the key initiating chemical reactions (e.g., Gerin et al. 2016). The reaction $\text{C}^+ + \text{H}_2(v) \rightarrow \text{CH}^+ + \text{H}$, for example, is endothermic by $E/k \simeq 4300$ K if $v=0$, but exothermic and fast for $v \geq 1$ (Hierl et al. 1997; Agúndez et al. 2010). Despite their short lifetimes, reactive ions can be detected and used to probe energetic processes in irradiated, circumstellar (e.g., Cernicharo et al. 1997), interstellar (e.g., Fuente et al. 2003), or protostellar (e.g., Benz et al. 2016) gas.

CO^+ and HOC^+ (the metastable isomer of HCO^+) have been detected in low angular resolution observations of UV-irradiated clouds near massive stars (Stoerzer et al. 1995; Apponi et al. 1999; Fuente et al. 2003). They are predicted to form close to the H/H_2 transition zone, the dissociation front (DF), by high-temperature reactions of C^+ with OH and H_2O , respectively (e.g., Sternberg & Dalgarno 1995). HOC^+ also forms by the reaction $\text{CO}^+ + \text{H}_2 \rightarrow \text{HOC}^+ + \text{H}$; thus, CO^+ and HOC^+ abundances are likely related (Smith et al. 2002). In photodissociation regions (PDRs), SO^+ is predicted to form primarily via the reaction $\text{S}^+ + \text{OH} \rightarrow \text{SO}^+ + \text{H}$ (e.g., Turner 1996). These ion-neutral reactions leading to CO^+ , HOC^+ and SO^+ are highly exothermic.

Herschel allowed the detection of OH, CH^+ , and SH^+ emission toward dense PDRs (Goicoechea et al. 2011; Nagy et al. 2013, 2017; Parikka et al. 2017). Unfortunately, the limited size of the space telescope did not permit us to resolve the $\Delta A_{\nu} \lesssim 1$ mag extent of the DF (a few arcsec for the closest PDRs). Therefore, the true spatial distribution of the reactive ions emission is mostly unknown. Unlike CH^+ , rotational lines of SH^+ can be observed from the ground (Müller et al. 2014). Here we report the first interferometric images of SH^+ , HOC^+ , and SO^+ .

The Orion Bar is a dense PDR (Hollenbach & Tielens 1999) illuminated by a far-UV (FUV) ($6 \text{ eV} < E < 13.6 \text{ eV}$) field of a few 10^4 times the mean interstellar radiation field. Because of its proximity (~ 414 pc, Menten et al. 2007) and nearly edge-on orientation, the Bar is a template to investigate the dynamics and chemistry in strongly FUV-irradiated gas (e.g., Pellegrini et al. 2009; Cuadrado et al. 2015; Goicoechea et al. 2016).

2 Observations and data reduction

The interferometric images were taken with the 7 m antennas of the Atacama Compact Array (ACA), Chile. The observations consisted of a 10-pointing mosaic centered at $\alpha(2000) = 5^{\text{h}}35^{\text{m}}20.6^{\text{s}}$; $\delta(2000) = -05^{\circ}25'20''$. The total field-of-view (FoV) is $\sim 50'' \times 50''$. Target line frequencies lie in the ~ 345 - 358 GHz range (Table A.1). Lines were observed with correlators providing ~ 500 kHz resolution over a 937.5 MHz bandwidth. The ALMA-

ACA observation time was ~ 6 h. In order to recover the extended emission filtered out by the interferometer, we used fully sampled single-dish maps as zero- and short-spacings. The required high-sensitivity maps were obtained using the ALMA total-power 12 m antennas ($\sim 19''$ resolution). We used the GILDAS/MAPPING software to create the short-spacing visibilities not sampled by ALMA-ACA. These visibilities were merged with the interferometric observations (Pety & Rodríguez-Fernández 2010). The dirty image was deconvolved using the Högbom CLEAN algorithm. The resulting cubes were scaled from Jy/beam to brightness temperature scale using the synthesized beam size of $4.9'' \times 3.0''$. The achieved rms noise is ~ 10 - 20 mK per 0.5 km s^{-1} smoothed channel, with an absolute flux accuracy of $\sim 10\%$. The resulting images are shown in Fig. 1.

In addition, we carried out pointed observations toward the DF with the IRAM 30m telescope (Spain). The observed position lies roughly at the center of the ALMA-ACA field (see circles in Fig. 1). This position is at $RA=+3''$ and $Dec=-3''$ from the “CO⁺ peak” of Stoerzer et al. (1995). These multi-line observations are part of a complete 80-360 GHz line survey at resolutions between $\sim 30''$ and $\sim 7''$ (Cuadrado et al. 2015).

3 Results: morphology and emission properties

In addition to the submillimeter (submm) emission images obtained with ALMA-ACA, panels b), c), and d) in Fig. 1 show images of the DF traced by the vibrationally excited molecular hydrogen (H_2^*) $v=1-0$ $S(1)$ line (Walmsley et al. 2000), of the atomic PDR (hydrogen is predominantly in neutral atomic form) as traced by the *Spitzer*/IRAC $8 \mu\text{m}$ emission (Megeath et al. 2012), and of the ionization front (IF), the H/H^+ transition zone. The δx axis shows the distance in arcsec to the IF. Thus, in each panel, the FUV-photon flux decreases from right to left.

The peak of the optically thick CO 3-2 line provides a good lower limit to the gas temperature in the molecular PDR ($\delta x > 15''$), with $T_k \gtrsim T_{\text{peak}}^{\text{CO}3-2} \simeq 150 \text{ K}$ (Fig. 1a). The ALMA-ACA images show that, except for SO^+ , the emission from reactive ions starts very close to the DF, and globally follows that of H_2^* . On small scales ($\lesssim 3'' \approx 1000 \text{ AU}$), several emission peaks of these ions coincide with the brightest H_2^* $v=1-0$ $S(1)$ peaks (e.g., at $\delta y \approx -18''$). Although the SH^+ and HOC^+ peaks at $\delta y \approx +27''$ do not exactly match a H_2 $v=1-0$ peak, observations do show the presence of extended H_2 $v=2-1$ and $1-0$ emission along the SH^+ and HOC^+ -emitting zone (van der Werf et al. 1996). In fact, H_2^* emission from very high vibrational levels (up to $v=10$ or $E/k \approx 50,000 \text{ K}$) has recently been reported (Kaplan et al. 2017).

To investigate the molecular emission stratification, in Fig. 2a we show averaged emission cuts perpendicular to the Bar. The cuts demonstrate that the SH^+ 1_0-0_1 and HOC^+ $4-3$ lines arise from a narrow emission layer (akin to a filament), with a half-power-width of $(\delta x) \approx 10''$ ($\approx 0.02 \text{ pc}$), that delineates the DF. The H^{13}CO^+ $4-3$ line displays this emission peak close to the DF, as well as another peak deeper inside the molecular cloud (at $\delta x \approx 30''$) that is dominated by emission from the colder molecular cloud interior. The SO 8_9-7_8 line arises from these more FUV-shielded zones. These spatial emission trends are supported by

the different line-widths (averaged over the ACA field of view, see Table A.1). In particular, the SO 8₉-7₈ line is narrower ($v=1.8\pm 0.1$ km s⁻¹) than the SO⁺ 15/2⁻-13/2⁺ ($v=2.1\pm 0.1$ km s⁻¹), HOC⁺ 4-3 ($v=2.7\pm 0.1$ km s⁻¹), and SH⁺ 1₀-0₁ ($v=2.8\pm 0.1$ km s⁻¹) lines that arise from the more FUV-irradiated gas near the molecular cloud edge.

We first derived H¹³CO⁺, HOC⁺, SO⁺, and SO rotational temperatures (T_{rot}) and column densities (N) by building rotational population diagrams from our IRAM 30m observations (line survey position, Cuadrado et al. 2015). Results are shown in Tables 1 and B.1. H¹³CO⁺ and HOC⁺ have high dipole moments (and SO⁺ to a lesser extent, but see Appendix D). Hence, the observed submm lines have moderate critical densities (several 10⁶ H₂ cm⁻³). The low- J transitions toward the line survey position are subthermal ($T_{\text{rot}} \approx 15$ K $\ll T_k$). Their column densities are relatively small: from $\sim 10^{11}$ cm⁻² (assuming uniform beam filling), to $\sim 10^{12}$ cm⁻² (for a more realistic filamentary emission layer of $\sim 10''$ width and correcting for beam dilution).

In addition, we estimated the average physical conditions that lead to the H¹³CO⁺, HOC⁺, SO⁺ and SH⁺ emission toward the line survey position. We used a Monte Carlo model (Appendix D) that includes inelastic collisions with H₂ and e⁻, as well as radiative excitation by the far-IR dust radiation field in the region (see Arab et al. 2012, and Fig. D.1). This allowed us to refine the source-averaged column density estimation for a 10''-wide emission layer (Table 1). The observed H¹³CO⁺, HOC⁺, and SO⁺ line intensities and T_{rot} are reproduced with $n(\text{H}_2) \approx 10^5$ cm⁻³, $n(e^-) = 10$ cm⁻³, and $T_k \gtrsim 200$ K (thus consistent with $T_{\text{peak}}^{\text{CO}3-2}$). However, with the set of assumed SH⁺ collisional rates, fitting the SH⁺ lines requires denser gas, $\sim 10^6$ cm⁻³ (see also Nagy et al. 2013). As T_k is expected to sharply vary along the DF (e.g., Sternberg & Dalgarno 1995), the result of these single-component models should be taken as average conditions (over the ACA resolution). We note that at the distance to Orion, 4'' is equivalent to 1 mag of visual extinction for $n_{\text{H}} = 10^5$ cm⁻³.

Low [HCO⁺]/[HOC⁺] abundance ratios (~ 200 -400) have previously been inferred from lower angular resolution (10'' to 70'', depending on the line and telescope) pointed observations toward the Bar (Apponi et al. 1999; Fuente et al. 2003). Such ratios are much lower than those predicted in FUV-shielded gas (>1000 , e.g., Goicoechea et al. 2009). Given the similar A_{ul} coefficient and upper level energy (E_{ul}/k) of the H¹³CO⁺ and HOC⁺ 4-3 transitions, their integrated intensity ratio is a good measure of the [HCO⁺]/[HOC⁺] isomeric ratio (lines are optically thin). The observed H¹³CO⁺/HOC⁺ 4-3 line ratio is equivalent to a roughly constant [HCO⁺]/[HOC⁺] ratio of 145 ± 5 along the $\delta x = 12$ -22'' layer (assuming [HCO⁺]/[H¹³CO⁺]=67). The ratio then increases as the FUV-photon flux decreases, [HCO⁺]/[HOC⁺]=180 \pm 4 along the $\delta x = 22$ -32'' layer, until the HOC⁺ 4-3 signal vanishes deeper inside the molecular cloud.

4 Discussion

ALMA HCO⁺ 4-3 images at $\sim 1''$ resolution suggest the presence of high-pressure structures, $P_{\text{th}}/k = n_{\text{H}} T_k \approx (1-2) \times 10^8$ K cm⁻³, close to the DF (Goicoechea et al. 2016). Despite the different resolutions, several of these HCO⁺ peaks coincide with the brightest

SH^+ 1_0-0_1 and OH $8_4 \mu\text{m}$ peaks (Figs. 1e and f). Thus, it is reasonable to assume that SH^+ arises from these structures.

We used version 1.5.2 of the Meudon PDR code (Le Petit et al. 2006) to model the formation and destruction of reactive ions in a constant thermal-pressure slab of FUV-irradiated gas (P_{th}/k from 2×10^7 to 2×10^8 K cm $^{-3}$). Figure 2b shows abundance profiles (with respect to H nuclei) predicted by the high-pressure model. The FUV-photon flux is $\chi=10^4$ (in Draine units), the expected radiation field close to the DF. Compared to Nagy et al. (2013), we have included more recent rates for reactions of S^+ with $\text{H}_2(\nu)$ (Zanchet et al. 2013). We adopt an undepleted sulfur abundance of $[\text{S}]=1.4 \times 10^{-5}$ (Asplund et al. 2005). The predicted abundance stratification in Fig. 2b qualitatively agrees with the observational intensity cut in Fig. 2a (but recall that the spatial scales are not directly comparable, as for the studied range of P_{th}/k in these 1D isobaric models, 10 mag of visual extinction corresponds to 1-10"). To be more specific, we compared the inferred column densities with those predicted by the PDR model (Table 1). Because the Orion Bar is not a perfect edge-on PDR, this comparison requires a knowledge of the tilt angle (α) with respect to a pure edge-on geometry, and of the line-of-sight cloud-depth (l_{depth}). Recent studies constrain α and l_{depth} to $\lesssim 4^\circ$ and ≈ 0.28 pc, respectively (Salgado et al. 2016; Andree-Labsch et al. 2017). For this geometry, the intrinsic width of the SH^+ - and HOC^+ -emitting layer would be narrower, from $\approx 10''$ (the observed value) to $\approx 2''$ (if the Bar is actually tilted). Given these uncertainties, the agreement between the range of observed and predicted columns is satisfactory for HOC^+ , H^{13}CO^+ , and SO^+ (Table 1). Although PDR models with lower pressures predict qualitatively similar stratification, and a reactive ion abundance peak also at $A_V \lesssim 1$ mag (where C^+ , S^+ , and H_2^+ coexist), a model with ten times lower P_{th} underestimates $N(\text{HOC}^+)$ and $N(\text{SO}^+)$ by large factors ($\gtrsim 20$). This is related to the lower predicted OH column densities (by a factor of ~ 25), key in the formation of CO^+ , HOC^+ and SO^+ (Goicoechea et al. 2011). Interestingly, SO^+ peaks deeper inside the cloud, while in the PDR models the main SO^+ peak is close to that of SH^+ . Compared to the other ions, SO^+ destruction near the DF is dominated by recombination and photodissociation (not by reactions with H_2 or H). Hence, $[\text{SO}^+]$ depends on the $[\text{OH}]/x_e$ ratio (Turner 1996) and on the photodissociation rate. The SO^+ line peaks deeper inside the cloud than the OH $2^2\Pi_{3/2} J=7/2^- - 5/2^+$ line (Fig. 1f) suggesting that near the DF either $n(e^-)$ is higher than in the model or, more likely, that the SO^+ photodissociation rate is larger. Indeed, SO^+ can be dissociated by lower E photons (< 5 eV, Bissantz et al. 1992). This process is not taken into account in the PDR model.

For SH^+ , we infer a column density that is a factor $\approx 3-30$ above the PDR model prediction (depending on α). Recall that reaction $\text{S}^+ + \text{H}_2(\nu) \rightarrow \text{SH}^+ + \text{H}$ (endothermic by $E/k \approx 9860$ K when $\nu=0$) only becomes exothermic when $\nu \geq 2$, but remains slow even then (Zanchet et al. 2013). The mismatch between model and observation, if relevant, may suggest an additional source of SH^+ that is not well captured by the model: overabundant $\text{H}_2(\nu \geq 2)$ or temperature/pressure spikes due to the PDR dynamics (Goicoechea et al. 2016).

Regardless of the excitation details, our observations show that detecting SH^+ and HOC^+ emission is an unambiguous indication of FUV-irradiated gas. Intriguingly, SH^+ and HOC^+ line-widths are narrower than those of CH^+ ($v \approx 4.5-5.5$ km s $^{-1}$, Nagy et al. 2013; Parikka et

al. 2017). The broader CH^+ lines in the Bar have been interpreted as a signature of CH^+ high reactivity (Nagy et al. 2013). In this view, the exothermicity (equivalent to an effective formation temperature of about 5360 K) of the dominant formation route, reaction $\text{C}^+ + \text{H}_2(v=1) \rightarrow \text{CH}^+ + \text{H}$, goes into CH^+ excitation and motion. However, reactive collisions of CH^+ with H and H_2 are faster than elastic and rotationally inelastic collisions (see Appendices C and D). In particular, the CH^+ lifetime is so short (a few hours) that the molecule does not have time to thermalize, by elastic collisions, its translational motions to a velocity distribution at T_k (Black 1998). Hence, the broad lines would be related to the energy excess upon CH^+ formation (thousands of K) and not to the actual T_k (at $T_k=1000$ K, the CH^+ thermal line-width will only be 1.8 km s^{-1} , Nagy et al. 2013), nor to an enhanced gas turbulence. Detailed models of the CH^+ excitation show that inclusion of formation and destruction rates in the level population determination affects the high- J levels (Godard & Cernicharo 2013). Indeed, using the CH^+ $J=3-2$ to $6-5$ intensities measured by *Herschel*/PACS toward the line survey position (Nagy et al. 2013), we derive $T_{\text{rot}}^{\text{PACS}} \simeq 150\text{K}$. This is significantly warmer than T_{rot} of SH^+ , HOC^+ and SO^+ .

CH^+ is a light hydride (see Gerin et al. 2016, for a review) meaning that its lowest rotational transitions lie at far-IR frequencies. Therefore, its critical densities are very high ($n_{\text{cr}}(\text{CH}^+ 4-3) \simeq 7 \times 10^9 \text{ H}_2 \text{ cm}^{-3}$, cf. $n_{\text{cr}}(\text{HOC}^+ 4-3) \simeq 4 \times 10^6 \text{ H}_2 \text{ cm}^{-3}$ at $T_k=200$ K). Such values are much higher than the gas density in the Orion Bar. Thus, without an excitation mechanism other than collisions, one would expect $T_{\text{rot}}(\text{CH}^+) \ll T_{\text{rot}}(\text{HOC}^+)$. However, CH^+ has a shorter lifetime than the other ions, and shorter than the timescale for inelastic

collisional excitations. Hence, the higher $T_{\text{rot}}^{\text{PACS}}(\text{CH}^+)$ compared to the heavier ions must be related to a formation, and perhaps radiative, pumping mechanism. In particular, the dust continuum emission is much stronger in the far-IR than in the (sub)mm (Fig. D.1). As a consequence, the far-IR CH^+ rotational transitions have larger radiative pumping rates than the (sub)mm transitions of the heavier ions. As an example, we derive

$$B_{3 \rightarrow 4} U_{3 \rightarrow 4}^{\text{Dust} + \text{CMB}}(\text{CH}^+) / B_{3 \rightarrow 4} U_{3 \rightarrow 4}^{\text{Dust} + \text{CMB}}(\text{HOC}^+) \approx 100$$

(where B_{lu} is the stimulated absorption coefficient and U is the energy density produced by the dust emission and by the cosmic background; see Appendix D.1). Therefore, CH^+ can be excited by radiation many times during its short lifetime (and during its mean-free-time for elastic collisions) so that it can remain kinetically hot (large velocity dispersion) and rotationally warm while it emits. On the other hand, the heavier ions are driven relatively faster toward smaller velocity dispersion by elastic collisions (narrower lines) and toward lower T_{rot} by inelastic collisions. For HOC^+ , we estimate that several collisional excitations take place during its lifetime (several hours). This subtle but important difference likely explains the narrower lines and lower T_{rot} of the heavier reactive ions, as well as their slightly different spatial distribution compared to CH^+ (see Fig. 1e).

Supplementary Material

Refer to Web version on PubMed Central for supplementary material.

Acknowledgements

We thank A. Parikka for sharing her *Herschel* far-IR CH⁺ and OH line maps. We thank the ERC for funding support under grant ERC-2013-Syg-610256-NANOCOSMOS, and the Spanish MINECO under grants AYA2012-32032, AYA2016-75066-C2-(1/2)-P and CSD2009-00038.

★★ Includes IRAM 30m telescope observations. IRAM is supported by INSU/CNRS (France), MPG (Germany), and IGN (Spain).

References

- Agúndez M, Goicoechea JR, Cernicharo J, Faure A, Roueff E. *ApJ*. 2010; 713:662.
- Andree-Labsch S, Ossenkopf-Okada V, Röllig M. *A&A*. 2017; 598:A2.
- Apponi AJ, Pesch TC, Ziurys LM. *ApJ*. 1999; 519:L89.
- Arab H, Abergel A, Habart E, et al. *A&A*. 2012; 541:A19.
- Asplund, M., Grevesse, N., Sauval, AJ. *Astronomical Society of the Pacific Conference Series*, Vol. 336, *Cosmic Abundances as Records of Stellar Evolution and Nucleosynthesis*. Barnes, TG., III, Bash, FN., editors. 2005. p. 25
- Benz AO, Bruderer S, van Dishoeck EF, et al. *A&A*. 2016; 590:A105.
- Bissantz H, Andric L, Hertzler C, Foth H-J, Linder F. *Zeitschrift für Physik D Atoms Molecules Clusters*. 1992; 22:727.
- Black JH. *Faraday Discussions*. 1998; 109:257.
- Cernicharo J, Liu X-W, González-Alfonso E, et al. *ApJ*. 1997; 483:L65.
- Cuadrado S, Goicoechea JR, Pilleri P, et al. *A&A*. 2015; 575:A82.
- Flower DR. *MNRAS*. 1999; 305:651.
- Fuente A, García-Burillo S, Usero A, et al. *A&A*. 2008; 492:675.
- Fuente A, Rodríguez-Franco A, García-Burillo S, Martín-Pintado J, Black JH. *A&A*. 2003; 406:899.
- Gerin M, Neufeld DA, Goicoechea JR. *ARA&A*. 2016; 54:181.
- Godard B, Cernicharo J. *A&A*. 2013; 550:A8.
- Goicoechea JR, Joblin C, Contursi A, et al. *A&A*. 2011; 530:L16.
- Goicoechea JR, Pety J, Cuadrado S, et al. *Nature*. 2016; 537:207. [PubMed: 27509859]
- Goicoechea JR, Pety J, Gerin M, et al. *A&A*. 2009; 498:771.
- Goicoechea JR, Pety J, Gerin M, et al. *A&A*. 2006; 456:565.
- Hierl PM, Morris RA, Viggiano AA. *J Chem Phys*. 1997; 106:10145.
- Hollenbach DJ, Tielens AGGM. *Rev Mod Phys*. 1999; 71:173.
- Kaplan KF, Dinerstein HL, Oh H, et al. *ArXiv e-prints*. 2017
- Le Petit F, Nehmé C, Le Bourlot J, Roueff E. *ApJS*. 2006; 164:506.
- Lique F, Spielfiedel A, Cernicharo J. *A&A*. 2006; 451:1125.
- Megeath ST, Gutermuth R, Muzerolle J, et al. *AJ*. 2012; 144:192.
- Menten KM, Reid MJ, Forbrich J, Brunthaler A. *A&A*. 2007; 474:515.
- Müller HSP, Goicoechea JR, Cernicharo J, et al. *A&A*. 2014; 569:L5.
- Nagy Z, Choi Y, Ossenkopf-Okada V, et al. *A&A*. 2017; 599:A22.
- Nagy Z, Van der Tak FFS, Ossenkopf V, et al. *A&A*. 2013; 550:A96.
- Parikka A, Habart E, Bernard-Salas J, et al. *A&A*. 2017; 599:A20.
- Pellegrini EW, Baldwin JA, Ferland GJ, Shaw G, Heathcote S. *ApJ*. 2009; 693:285.
- Pety J, Rodríguez-Fernández N. *A&A*. 2010; 517:A12.
- Salgado F, Berné O, Adams JD, et al. *ApJ*. 2016; 830:118.
- Smith MA, Schlemmer S, von Richthofen J, Gerlich D. *ApJ*. 2002; 578:L87.
- Sternberg A, Dalgarno A. *ApJS*. 1995; 99:565.
- Stoerzer H, Stutzki J, Sternberg A. *A&A*. 1995; 296:L9.
- Turner BE. *ApJ*. 1996; 468:694.

- van der Werf PP, Stutzki J, Sternberg A, Krabbe A. *A&A*. 1996; 313:633.
Walmsley CM, Natta A, Oliva E, Testi L. *A&A*. 2000; 364:301.
Zanchet A, Agúndez M, Herrero VJ, Aguado A, Roncero O. *AJ*. 2013; 146:125.

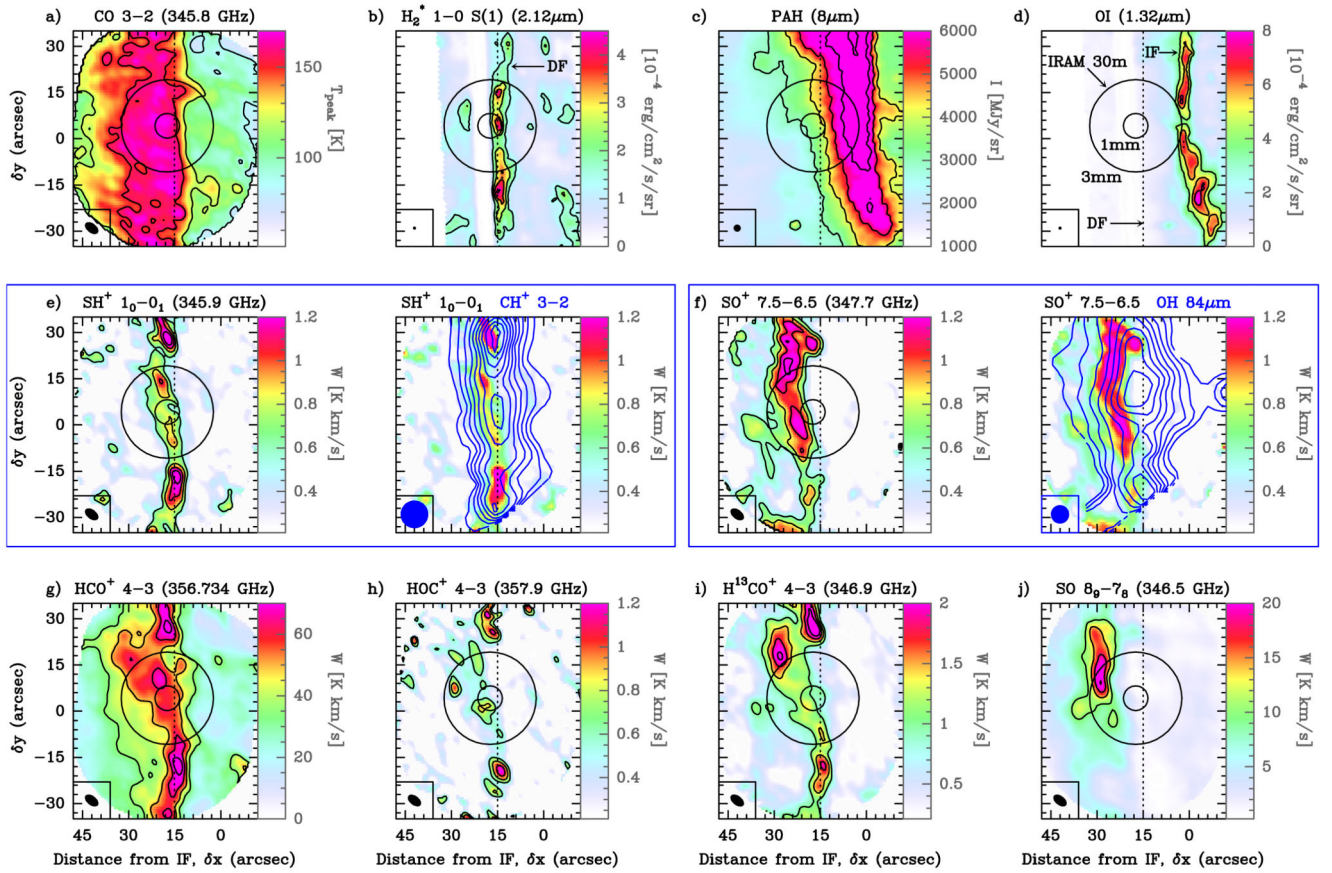


Fig. 1.

ALMA-ACA and complementary images of the Bar. All images have been rotated to bring the FUV illuminating direction roughly in the horizontal direction (from the right). The circles indicate the position of our IRAM 30 m line survey, with beams of $\approx 8''$ ($\approx 30''$) at 1 mm (3 mm). The upper row shows images of b) the H_2 $v=1-0$ $S(1)$ line at $2.12 \mu\text{m}$, delineating the DF (Walmsley et al. 2000), c) the Spitzer $8 \mu\text{m}$ emission produced mainly by PAHs (Megeath et al. 2012), and d) the fluorescent O_I line at $1.32 \mu\text{m}$ at the H_{II} /PDR boundary (Walmsley et al. 2000). The blue contours in e) and f) represent the CH^+ $119.8 \mu\text{m}$ ($\approx 9''$ resolution) and OH $84.6 \mu\text{m}$ ($\approx 6''$) lines mapped by *Herschel* (Parikka et al. 2017).

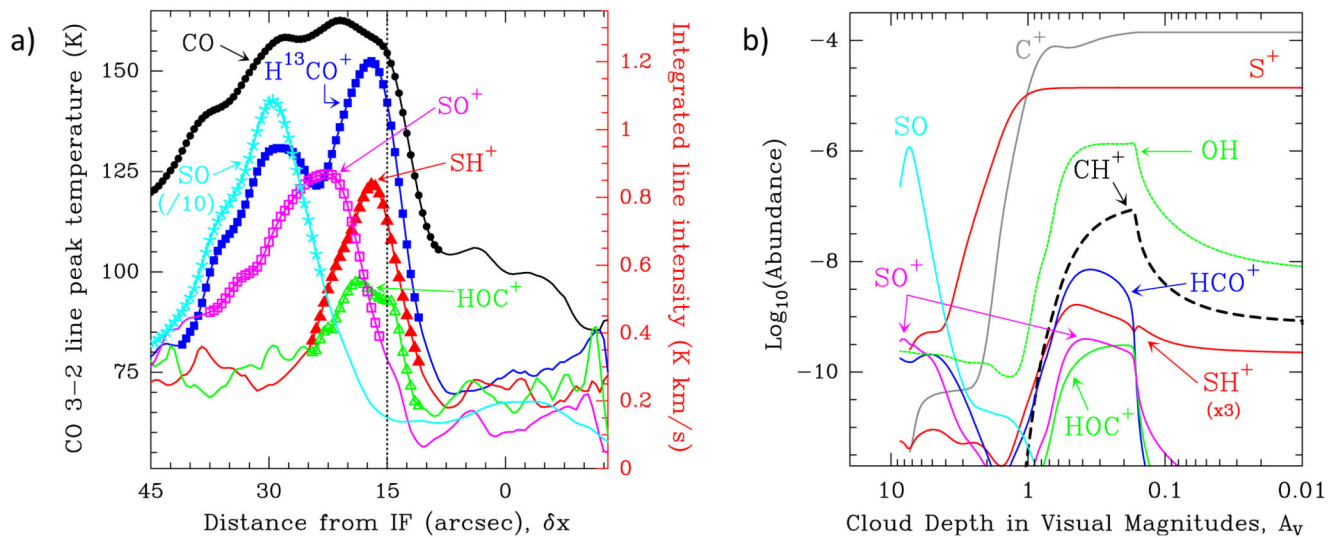


Fig. 2.

a) ALMA-ACA averaged intensity cuts perpendicular to the Orion Bar. Except for CO $J=3-2$ line (peak temperature in K), cuts show integrated line intensities (in K km s^{-1}). Symbols do not have any meaning, they are used to improve Figure readability. b) Isobaric model of a PDR with $P_{\text{th}}/k=2\times 10^8 \text{ K cm}^{-3}$ and $\chi=10^4$. In both Figures, the FUV radiation from the Trapezium cluster comes from the right-hand side.

Table 1

Inferred column densities and PDR model predictions.

	$\log_{10} N [\text{cm}^{-2}]$	Rotational Diagram	Non-LTE [†]	PDR Model [‡]
H ¹³ CO ⁺	11.8 ^a - 12.1 ^b		12.3	11.0 ^c - 12.2 ^d
HOC ⁺	11.6 ^a - 11.9 ^b		12.0	11.7 ^c - 12.9 ^d
SO ⁺	12.3 ^a - 12.5 ^b		12.5	12.4 ^c - 13.5 ^d
SH ⁺	–		13.2	11.7 ^c - 12.8 ^d

Notes.[†]From a non-LTE model.[‡]Isobaric PDR model ($P_{\text{H}}/k=2 \cdot 10^8 \text{ K cm}^{-3}$ and $\chi=10^4$). Columns integrated up to $A \nu=10$.^aAssuming uniform beam filling.^bFor a filament of 10'' -width.^cFace-on geometry.^dEdge-on geometry with a tilt angle of $\alpha \approx 4^\circ$.